# Motion-Model-Based Boundary Extraction

Hongche Liu[†‡], Tsai-Hong Hong[‡], Martin Herman[‡], and Rama Chellappa[†]

liu@cme.nist.gov, hongt@cme.nist.gov, herman@cme.nist.gov, chella@eng.umd.edu

[‡]NIST, Intelligent Systems Division, Bldg 220, Rm B124, Gaithersburg, MD 20899
[†]Center for Automation Research, University of Maryland, College Park 20742

## Abstract

*Motion boundary extraction and optical flow computation are two subproblems of the motion recovery problem that cannot be solved independently of one another. We present a local, non-iterative algorithm that extracts motion boundaries and computes optical flow simultaneously. This is achieved by modeling a 3-D image intensity block with a general motion model that presumes locally coherent motion. Local motion coherence, which is measured by the fitness of the motion model, is the criterion we use to determine whether motion should be estimated. If not, then motion boundaries should be located. The motion boundary extraction algorithm is evaluated quantitatively and qualitatively against other existing algorithms in a scheme originally developed for edge detection.*

## 1. Introduction

In this paper, the problem of *motion recovery* is referred to as involving two major subproblems: *optical flow computation* and *motion segmentation*. Optical flow computation quantitatively measures the motion associated with the perceived objects; motion segmentation, on the other hand, qualitatively distinguishes different moving objects. The fact that they are dependent on each other has complicated the general motion recovery problem.

Due to the aperture problem, early motion estimation algorithms [15][16]usually enforced a smooth flow field as an additional constraint. Recent approaches use spatiotemporal filters [8][12][20], often with large support, to estimate image properties and then solve for optical flow. In either case, on or near motion boundaries, this smoothing or filtering renders the estimation incorrect. In other words, motion estimation is not accurate until we know where the boundaries are. On the other hand, motion boundaries are defined as motion field discontinuities. Due to optical flow error around motion boundaries, the requirement of a dense flow field, and noise in the optical flow field, motion boundaries are very difficult to extract and/or locate from optical flow. Researchers have used other image cues, for example, accretion and deletion[23], or normal flow [15], to detect motion discontinuities, but they are not always correct because they provide only partial information about the motion. In other words, motion boundaries cannot be located accurately without a dense and accurate optical flow field.

Even though they are two aspects of a single problem, optical flow computation has received much more attention in the literature than motion boundary extraction. Existing methods for motion boundary extraction are approached through optical flow algorithms. A popular technique is to use an iterative scheme that consists of two components: optical flow estimation and motion boundary extraction. The basic idea is to refine both components' results through iteration. This approach is time-consuming and sometimes does not converge.

"Global" motion segmentation is one approach to the problem. In our approach, however, "local" motion boundary extraction can be combined with optical flow in an algorithm for motion recovery. Our view is that local image properties provide abundant information and motion recovery should be performed locally[19].

The local image properties we use are image derivatives. With the aid of sufficient and accurate image derivatives, a motion-model-based approach to boundary extraction becomes possible. We describe a general motion model and derive linear motion equations in terms of image derivatives. Pixels whose image derivatives fit the model are locations where the motion is coherent, so the motion can be estimated using the linear system. Those pixels that do not fit the model represent failures of the motion model in describing the local motion. A failure of the model can best be attributed to multiple motions or motion boundaries existing in the local window used to estimate the image properties. Using a least square error method on the overdetermined linear system, a failure of the model is measured by the residual. An analysis of the residual is shown to reflect the likelihood of a motion boundary.

Using the residual for motion boundary extraction offers several advantages over using flow. First, since the residual is a scalar, it avoids the difficulty of handling vector field discontinuities, yet provides equivalent information about

motion boundaries. Second, flow values on boundaries are not accurate and are very noisy, and thus require smoothing for boundary extraction. This extra smoothing may cause localization error. Third, the residual is computed using a 3-D motion model so that it corresponds to real motion boundaries and is not susceptible to nonuniformity (e.g., affinity) of flow within an object.

The appeal of a local, non-iterative approach lies in its potential speed. However, its accuracy should not be compromised. To measure the accuracy, we need an evaluation scheme to compare different motion boundary extraction algorithms. Since many recent approaches combine optical flow and motion boundary detection, evaluation has often been performed based on the final optical flow. This has the disadvantage of not distinguishing the source of error, which may be due to inaccurate optical flow or inaccurate motion boundary location. In other words, evaluation based on segmented optical flow does not suggest a direction for improvement. Hence, we apply here a quantitative evaluation scheme only to motion boundary extraction. This scheme was originally developed for edge detection [14]. The results will demonstrate that our algorithm locates boundaries more accurately than two representative existing algorithms.

## 2. Previous Work

Braddick's psychological experiments on random dot motion [4] set the stage for vision research on motion boundaries. It verified the human visual capability of perceiving motion boundaries clearly without any other visual cues such as texture. Table 1 summarizes the existing work on motion boundary extraction or segmentation. A detailed comparisons of these methods can be found in [21].

Early research on motion boundary extraction or motion segmentation can be roughly characterized as based on a non-iterative approach. These algorithms can be put into three categories [7][28] based on whether the motion boundary extraction is performed prior to, simultaneously with, or after the flow field estimation (Refer to Table 1).

The iterative method for motion recovery is an approach developed more recently. It has both optical flow estimation and segmentation components. These components interact with each other and improve their individual results during the course of the iteration. Pyramid linking, Markov random fields with line processes, tracking plus nulling techniques, and robust estimation have been proposed (Refer to Table 1). Iterative methods tend to be more accurate than non-iterative methods, but they have two major problems. The first is the high computational load; the second is that the convergence rate depends on the scene, noise, and motion. Moreover, some of these algorithms may not converge at all.

## 3. Motion-Model-Based Boundary Extraction

The basic idea of our motion-model-based boundary extraction method is to fit the local image properties with a general motion model. The necessary elements of the scheme are a general motion model which is based on arbitrary 3-D motion; an accurate estimate of image properties, for which we use image spatio-temporal derivatives; and a procedure to measure the fitness of the image properties to the motion model. The following subsections briefly present the derivations of these three elements; the details can be found in [19]and [20].

### 3.1 The general motion model

Here we describe an image motion model and an image motion equation that relates the spatio-temporal derivatives of the image intensity patterns in a sequence. Let a 3-D point $\dot{P} = (X, Y, Z)^T$ in the scene undergo steady small rotation $(\Omega_X, \Omega_Y, \Omega_Z)$ and translation $(T_X, T_Y, T_Z)$ per unit time. Using the 3-D motion transformation matrix $M$

$$\begin{bmatrix} X' \\ Y' \\ Z' \\ 1 \end{bmatrix} = M \begin{bmatrix} X \\ Y \\ Z \\ 1 \end{bmatrix}, \text{ where } M = \begin{bmatrix} 1 & -\Omega_Z & \Omega_Y & T_X \\ \Omega_Z & 1 & -\Omega_X & T_Y \\ -\Omega_Y & \Omega_X & 1 & T_Z \\ 0 & 0 & 0 & 1 \end{bmatrix}, \quad (1)$$

**Table 1 Summary of current motion boundary extraction algorithms**

| Non-iterative schemes | | Iterative schemes | |
|---|---|---|---|
| **Motion boundary extraction vs. flow estimation** | **Algorithm by** | **Technique** | **Algorithm by** |
| Prior to | Hildreth [15], Spoerri & Ullman [28] | Pyramid linking | Hartley [10] |
| Simultaneous with | Mutch & Thompson [23], Schunck [26], Shizawa & Mase [27] | Markov random field with binary line processes | Koch, Marroquin & Yuille [18], Murray & Buxton [22], Heitz & Bouthemy [13] |
| After | Potter [25], Nakayama & Loomis [24], Adiv [1], Thompson, Mutch, & Berzins [29], Dengler [7] | Tracking & nulling | Bergen, et al. [3] |
| | | Robust estimation | Darrel & Pentland [6], Jepson & Black [17] |

$$\text{and} \quad \begin{bmatrix} \dot{P}(t) \\ 1 \end{bmatrix} = M^t \begin{bmatrix} \dot{P}(0) \\ 1 \end{bmatrix} . \qquad (2)$$

Under perspective projection with focal length $f$ and with the small motion assumption, we arrive at the image motion equation (3) from the brightness constancy relation, i.e., $I(x(t), y(t), t) = I(x_0, y_0, 0) = F(x_0, y_0)$ ,

$$I(x, y, t) = F(x + t(\alpha + \gamma x + \rho y + \delta x^2 + \varepsilon xy) \qquad (3)$$
$$, y + t(\beta - \rho x + \gamma y + \delta xy + \varepsilon y^2))$$

where $\alpha = -f\left(\frac{T_X}{Z} + \Omega_Y\right), \beta = -f\left(\frac{T_Y}{Z} - \Omega_X\right).$ (4)

$$\gamma = \frac{T_Z}{Z}, \rho = \Omega_Z, \delta = -\frac{1}{f}\Omega_Y, \varepsilon = \frac{1}{f}\Omega_X$$

For a detailed derivation, refer to [19]. From this equation, we see that the image motion is quadratic with respect to local coordinates. However, it is linear in terms of the six motion parameters $\alpha, \beta, \gamma, \rho, \delta, \varepsilon$. To further simplify, we assume small rotation and reasonably long focal length. Equation (3) reduces to a linear image motion model with four motion parameters $\alpha, \beta, \gamma, \rho$,

$$I(x, y, t) = F(x + t(\alpha + \gamma x + \rho y), y + t(\beta - \rho x + \gamma y)) \quad . (5)$$

Note that $(\alpha, \beta)$ are related to image flow, $\gamma$ to divergence and $\rho$ to curl. Equation (5) will be used in the following derivation.

### 3.2 Hermite polynomial differentiation filters

The $n$th Hermite polynomial $H_n(x)$ is a solution of

$$\frac{d^2 H_n}{dx^2} - 2x\frac{dH_n}{dx} + 2nH_n = 0. \qquad (6)$$

The $H_n(x)$ are derived by Rodrigues' formula [11]

$$H_n(x) = (-1)^n e^{x^2} \frac{d^n}{dx^n} e^{-x^2} . \qquad (7)$$

By substituting $G(x)$ (with variance $\sigma^2$) for $e^{-x^2}$ in (7), we generalize to Hermite polynomials with respect to the Gaussian function. Let these Hermite polynomials be denoted by $\bar{H}_n(x)$. The scalar product of two functions and the $L_2$-norm of a function with *G(x)* as a weight function are defined as:

$$\langle a, b \rangle \equiv \int_{-\infty}^{\infty} G(x)a(x)b(x)dx \quad \text{and } \|a\| \equiv \langle a, a \rangle^{1/2}. \quad (8)$$

The orthogonality of $\{ \bar{H}_n(x) \}$ can be expressed in the following way[11]:

$$\langle \bar{H}_m, \bar{H}_n \rangle = \sigma^{-2n} n! \delta_{mn}, \qquad (9)$$

The 3D case of Hermite polynomials is especially simple because they are separable:

$$\bar{H}_{ijk}(x, y, t) = \bar{H}_i(x) \cdot \bar{H}_j(y) \cdot \bar{H}_k(t) \qquad (10)$$

We use the following Gaussian derivative theorem to derive motion constraint equations.

Theorem 1: A one dimensional signal $I(x)$ can be expanded in terms of Hermite polynomials as

$$I(x) = \sum_{k=0}^{\infty} I_k \frac{\bar{H}_k(x)}{\|\bar{H}_k\|^2} \qquad (11)$$

Then $I_k = \langle I, \bar{H}_k \rangle = \langle I^{(k)}, \bar{H}_0 \rangle$, where $I^{(k)} = \frac{d^k I}{dx^k}$.

Expand both sides of equation (5) with Hermite polynomials,

$$\sum_{i=0}^{\infty}\sum_{j=0}^{\infty}\sum_{k=0}^{\infty} I_{ijk} \frac{\bar{H}_{ijk}}{\|\bar{H}_{ijk}\|^2} = \sum_{i=0}^{\infty}\sum_{j=0}^{\infty}\sum_{k=0}^{\infty} F_{ijk} \frac{\bar{H}_{ijk}}{\|\bar{H}_{ijk}\|^2} \text{ then}$$

$$I_{ijk} = \langle I, \bar{H}_{ijk} \rangle = F_{ijk} = \langle F, \bar{H}_{ijk} \rangle \qquad (12)$$

Equating $I_{ij1}$ to $F_{ij1}$ and using Theorem 1, we derive (see [19] for details)

$$I_{ij1} \approx \alpha I_{(i+1)j0} + \beta I_{i(j+1)0} + \gamma(i + j)I_{ij0} \quad . \quad (13)$$
$$+ \rho(iI_{(i+1)(j-1)0} + jI_{(i-1)(j+1)0})$$
$$+ \gamma\sigma^2(I_{(i+2)j0} + I_{i(j+2)0}) + \rho\sigma^2 I_{(i+1)(j+1)0}$$

Neglecting higher order Gaussian derivatives due to their relatively small magnitude and potential inaccuracy, we further simplify to

$$I_{ij1} \approx \alpha I_{(i+1)j0} + \beta I_{i(j+1)0} + \gamma(i + j)I_{ij0} \qquad (14)$$
$$+ \rho(iI_{(i+1)(j-1)0} + jI_{(i-1)(j+1)0})$$

We use motion equation (14) in a linear least square formulation,

$$E = min\|As + b\|, \text{ where } s = (\alpha, \beta, \gamma, \rho) ; A \text{ and } b$$
consist of image spatio-temporal derivatives. (15)

It is necessary that we derive the motion constraint equations up to the third order for the purpose of motion boundary extraction because we need to have more constraints than unknowns to obtain a least square formulation and compute the residual, $E$ in (15). Since the 3-D Hermite polynomial filters are orthogonal Gaussian derivatives, they are very stable up to this order.

### 3.3 Residual for boundary extraction

The residual measures the amount of disagreement among the equations in a linear system. If these equations are derived from a mathematical model, then the residual reflects the deviation from the underlying assumptions of the model. In our case, the assumptions are brightness con-

stancy and local coherent motion. Our motion boundary extraction algorithm is based on the analysis of the relationship between the residual and the motion boundary.

The residual of our algorithm is $E = min\|As + b\|$. The residual error results from the approximation errors of our computational model in describing the physical world. Specifically, these errors are:

1. The assumption of the motion model is violated in the local window, i.e., the window covers more than one moving object.
2. The assumption of constant image brightness is violated, i.e., the image intensity pattern changes over time due to sensor noise, change in the viewing angle, shadows, etc.
3. Quantization errors result from digitization of the image intensities and sampling of the Hermite polynomial filters. Truncation errors are introduced when we use a limited spatial support to compute $\{I_{ijk}\}$. This situation is worse for higher order differentiation filters.

Hence we can model the above errors as perturbations or noise to the linear system [20]:

$$\tilde{E} = min\|(A+N)\tilde{s} + (b+\Delta b)\| \text{ , where } N \text{ and } \Delta b \text{ denote errors in the filter output.} \quad (16)$$

We derive the analytical relationship between the residual and the errors as follows. Let $A$ and $b$, defined in (15), contain no noise. Then

$$E = As + b = 0 \text{ and } s = -(A^TA)^{-1}A^Tb. \quad (17)$$

Let the noise contaminated optical flow be $\tilde{s}$ and the new residual be $\tilde{E}$, and assume that $N \ll A$ and $\Delta b \ll b$ elementwise, i.e., $NN^T = 0$ and $N\Delta b = 0$. Then

$$\tilde{s} = -[(A+N)^T(A+N)]^{-1}(A+N)^T(b+\Delta b) \quad , \quad (18)$$

$$[(A+N)^T(A+N)]^{-1} \approx (A^TA[I + (A^TA)^{-1}(A^TN + N^TA)])^{-1}$$
$$\approx [I - (A^TA)^{-1}(A^TN + N^TA)](A^TA)^{-1} \quad (19)$$

From (18) and (19), we derive

$$\tilde{s} \approx -(A^TA)^{-1}A^Tb + (A^TA)^{-1}(A^TN + N^TA)(A^TA)^{-1}A^Tb - (A^TA)^{-1}N^Tb - (A^TA)^{-1}A^T\Delta b \quad (20)$$

Using (17), we derive

$$\Delta s = s - \tilde{s} \approx (A^TA)^{-1}A^TNs + (A^TA)^{-1}A^T\Delta b. \quad (21)$$

Substituting $\tilde{s}$ into (16), and using (17), we derive

$$\tilde{E} \approx \|(A+N)s - A(A^TA)^{-1}A^TNs - A(A^TA)^{-1}A^T\Delta b + b + \Delta b\|$$
$$\approx \|(I - A(A^TA)^{-1}A^T)(Ns + \Delta b)\| \quad (22)$$

Further analysis shows that the expression $I - A(A^TA)^{-1}A^T$, denoted by $T$, has only two nontrivial eigenvalues, both 1. We thus conclude that $\tilde{E}$ is proportional to the noise magnitude.

But in order to use the residual to extract boundaries we still need to separate the residual error induced by motion boundaries from that by other sources. To do this, we observe the residual profile, as explained below.

Fig 1.1 shows a motion boundary neighborhood. A

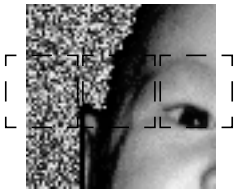

**Fig 1.1 Sliding window across boundary**

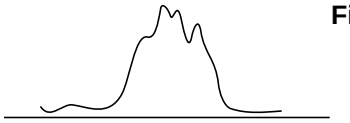

**Fig 1.2 Typical residual profile across boundary**

dashed square represents a local window used to estimate image derivatives and the residual for the center pixel. By sliding the window across the boundary, we can compute and plot the residual profile. A typical residual profile is shown in Fig 1.2. It has a plateau centered around the motion boundary because only in that plateau region does the local window cover the boundary.

Brightness changes and quantization errors, on the other hand, are usually scattered in the image and not likely to output residual profiles similar to those of motion boundaries. Also, since residuals arising from motion boundaries are usually larger than those arising from the other two sources, their profiles should be very prominent.

Based on the above findings, we can extract motion boundaries using spatial filters designed according to Canny's criteria [5] for wide ridge edge detection. The maxima of the two responses are thresholded to form thick boundaries. On the thick boundaries, we perform a morphological medial axis operation or skeletonization[9] to extract the center loci of the boundaries. Some simple pruning and contour following are then done to prevent streaking.

## 4. Experiments, Evaluations and Conclusion

It is important to evaluate motion boundary extraction separately from optical flow. It makes clear what component of the motion recovery algorithm needs improving.

We use Heyden's quantitative method of evaluation [14] because it offers several advantages: first, it penalizes long streaking, i.e., large gaps of missed boundaries; second, it penalizes thick edges; third, there is no need to perform a search for correspondences between detected and ground truth motion boundaries. In this scheme, a smaller performance measure represents a better result, with zero as the minimum.

In order to make comparisons, we also implemented algorithms developed by Schunck [26] and Thompson, et al.

[29]. In implementing Schunck's algorithm, we used 3-D Hermite polynomial filters to compute first order derivatives and perform constraint line clustering to estimate optical flow. The Canny edge detector is applied to the flow components to find motion boundaries. In implementing Thompson's algorithm, we used Lucas & Kanade's algorithm implemented by Barron, et al. [2]. The initial flow output is not dense, so we implemented a propagation and smoothing technique to fill the field. We then use the vector field discontinuity detector suggested in [29], i.e., direction reversal of the Laplacian response of the flow vector field, to locate motion boundaries.

Fig 2.1 shows the first image we used. It is a sequence

**Fig 2.1 Moving face on random dots**

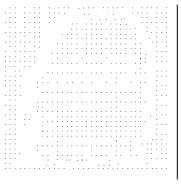

**Fig 2.2 Approximate flow field**

**Fig 2.3 Motion boundary**

composed of a baby face traversing laterally in front of a moving random dot background. The approximate flow map and the motion boundary ground truth are shown in Fig 2.2 and Fig 2.3, respectively. This image sequence is synthesized so as to contain curved motion boundaries, which are common in real world scenes but present difficulties for motion boundary extraction algorithms.

Fig 3.1-Fig 3.3 show our algorithm's residual map and Schunck's and Thompson's flow fields. They represent the bases upon which these algorithms extract boundaries. Th-

**Fig 3.1 Residual map**

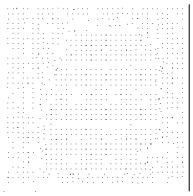

**Fig 3.2 Schunck's flow field**

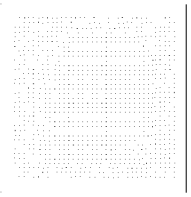

**Fig 3.3 Thompson's flow field**

ompson's flow field (Fig 3.3) is smooth across boundaries as expected, while Schunck's flow field (Fig 3.2) is noisier right on boundaries but more accurate near boundaries.

Next we show the detected boundary and true motion boundary for the three algorithms. In Fig 4.1-Fig 4.3, the dark edge represents the true motion boundary while the white edge represents the detected boundary. These images are obtained by subtracting the ground truth boundary image from the detected boundary image as dictated by Heyden's evaluation scheme.

**Fig 4.1 Our algorithm's boundary**

**Fig 4.2 Schunck's boundary**

**Fig 4.3 Thompson's boundary**

In Fig 4.2, it can be seen that Schunck's algorithm suffers from boundary drift caused by noise on the boundary as well as localization errors in the corners, as mentioned in [26]. On the other hand, when the motion boundary is a straight line, Schunck's algorithm performs better than the other two. In Fig 4.3, it can be seen that Thompson's algorithm suffers from flow noise away from boundaries. Since it uses a direction reversal technique similar to zero crossings, spurious edges are detected. Otherwise, the localization is very good. Our algorithm's boundary is better at corners and essentially free of the major problems of the other two. Table 2 summarizes the quantitative performance measure computed by Heyden's evaluation scheme and shows that our algorithm is better than the other two.

**Table 2 Summary of quantitative performance measure**

| Comparison Algorithms | Our Algorithm | Schunck's Algorithm | Thompson's Algorithm |
|---|---|---|---|
| Performance measure | 5.85 | 7.86 | 10.32 |

The next image we use is the Yosemite fly-by sequence in which two prominent motion boundary curves exist. One separates the sky from the mountains, and the other separates the domed mountain in the lower left corner from the other mountains. The boundary ground truth is not available. Fig 5.1-Fig 5.3 show the results of the three boundary extraction algorithms overlaid on the original image. The white edge points represent the extracted boundaries.

**Fig 5.1 Our algorithm's result**

**Fig 5.2 Schunck's result**

**Fig 5.3 Thompson's result**

Note that the boundaries that separate sky and mountains are easier to extract because the motion directions are different on the two sides. All three algorithms indeed extract these boundaries. However, the other boundary is not as easy to extract because the motions on the two sides are

in the same direction but have different magnitudes. Note that this kind of motion field is typical in image sequences captured by a forward moving observer. In Fig 5.2 Schunck's algorithm fails to extract these boundaries because the noise on both sides overwhelms the small variation in flow. In Fig 5.3 Thompson's algorithm fails to extract these boundaries because the presmoothing and filling of the sparse field smooths out the small flow variation. On the other hand, our algorithm extracts a large part of this boundary curve (Fig 5.1).

Our method offers the capability of segmenting moving objects with not only different flows, but also different divergences (e.g. in the Yosemite sequence), or curls. This is because in our general motion model formulation, the residual values account for incoherence in flow $(\alpha, \beta)$, divergence $\gamma$ and curl $\rho$.

## References


[1] Adiv, G., "Inherent Ambiguities in Recovering 3-D Motion and Structure from a Noisy Flow Field", IEEE Transactions on Pattern Analysis and Machine Intelligence, vol. 11, no. 5, pp. 477-489, 1989.

[2] Barron, J. L., Fleet, D. J. and Beauchemin, S. S., "Performance of Optical Flow Techniques", International Journal of Computer Vision, vol. 12, no. 1, pp. 43-77, 1994.

[3] Bergen, J., Burt, P., Hingorani, R. and Peleg, S., "A Three-Frame Algorithm for Estimating Two-Component Image Motion", IEEE Transactions on Pattern Recognition and Machine Intelligence, vol. 14, no.9, pp. 886-896, 1992.

[4] Braddick, O.J., "A Short-Range Process in Apparent Motion", Vision Research, vol. 14, pp. 519-527, 1974.

[5] Canny, J., "A Computational Approach to Edge Detection", IEEE Transactions on Pattern Recognition and Machine Intelligence, vol. 8, no.11, pp. 679-698, 1986.

[6] Darrel, T. and Pentland, A., "Robust Estimation of a Multi-Layered Motion Representation", Proceedings of IEEE Workshop on Visual Motion, Princeton, NJ, pp. 173-178, 1991.

[7] Dengler, J., "Estimation of Discontinuous Displacement Vector Fields with the Minimum Description Length Criterion", Proceedings of the IEEE Conference on Computer Vision and Pattern Recognition, Lahaina, HI, pp. 276-282, 1991.

[8] Fleet, D.J. and Jepson, A.L., "Computation of Component Image Velocity from Local Phase Information", International Journal of Computer Vision, vol. 5, no.1, pp. 77-104, 1990.

[9] Giardina, C. and Dougherty, E.R., "Morphological Methods in Image and Signal Processing", Prentice Hall, Englewood Cliffs, NJ, 1988.

[10] Hartley, R., "Segmentation of Optical Flow Fields by Pyramid Linking", Pattern Recognition Letters, vol.3, no. 5, pp.253-262, 1985.

[11] Hashimoto M. and Sklansky, J. "Multiple-Order Derivatives for Detecting Local Image Characteristics", Computer Vision, Graphics, and Image Processing, vol. 39, pp. 28-55, 1987.

[12] Heeger, D. J., "Optical Flow Using Spatiotemporal Filters", International Journal of Computer Vision, vol. 1, no. 4, pp. 279-302, 1988.

[13] Heitz, F. and Bouthemy, P., "Multimodal Estimation of Discontinuous Optical Flow Using Markov Ransom Fields", IEEE Transactions on Pattern Recognition and Machine Intelligence, vol. 15, no.12, pp. 1217-1232, 1993.

[14] Heyden, F., "Evaluation of Edge Detection Algorithms", Proceedings of the IEEE Conference on Computer Vision and Pattern Recognition, pp.618-622, 1992.

[15] Hildreth, E., "The Measurement of Visual Motion", MIT Press, Cambridge, MA, 1984.

[16] Horn, B. K. P. and Schunck, B. G., "Determining Optical Flow", Artificial Intelligence, vol. 17, pp. 185-204, 1981.

[17] Jepson, A., Black, M., "Mixture Model for Optical Flow Computation", Proceedings of IEEE Conference on Computer Vision and Pattern Recognition, New York, NY, pp.760-761, 1993.

[18] Koch, C., Marroquin, J. and Yuille, A., "Analog 'Neural' Networks in Early Vision", Proceedings of the National Academy of Sciences, vol. 83, pp. 4263-4267, 1986.

[19] Liu, H., Hong, T., Herman, M. and Chellappa, R., "A Generalized Motion Model for Estimating Optical Flow Using 3-D Hermite Polynomials", Proceedings of the International Conference on Pattern Recognition, Jerusalem, Israel, pp. 360-366, 1994.

[20] Liu, H., Hong, T., Herman, M. and Chellappa, R., "A General Motion Model and Spatio-temporal Filters for Computing Optical Flow", University of Maryland-TR -3365, November 1994.

[21] Liu, H., Hong, T., Herman, M. and Chellappa, R., "Motion-Model-Based Boundary Extraction", University of Maryland TR-3414, February, 1995.

[22] Murray, D. and Buxton, B., "Scene Segmentation from Visual Motion Using Global Optimization", IEEE Transactions on Pattern Recognition and Machine Intelligence, vol. 9, no.2, pp. 220-228, 1987.

[23] Mutch, K. and Thompson, W., "Analysis of Accretion and Deletion at Boundaries in Dynamic Scenes", IEEE Transactions on Pattern Recognition and Machine Intelligence, vol. 7, no.2, pp. 133-138, 1985.

[24] Nakayama, K. and Loomis, J.M., "Optical Velocity Patterns, Velocity Sensitive Neurons, and Space Perception: a Hypothesis", Perception, vol. 3, 1974.

[25] Potter, J. L., "Velocity as a Cue to Segmentation Using Motion Information", IEEE Transactions on Systems, Man, Cybernetics, vol. 5, pp. 390-395, 1975.

[26] Schunck, B., "Image Flow Segmentation and Estimation by Constraint Line Clustering", IEEE Transactions on Pattern Recognition and Machine Intelligence, vol. 11, no.10, pp. 1010-1027, 1989.

[27] Shizawa, M. and Mase, K., "A Unified Computational Theory for Motion Transparency and Motion Boundaries Based on Eigenenergy Analysis", Proceedings of the IEEE Conference on Computer Vision and Pattern Recognition, Lahaina, HI, pp. 289-295, 1991.

[28] Spoerri, A. and Ullman, S., "The Early Detection of Motion Boundaries", A.I. Memo no. 935, AI Lab, MIT, 1987.

[29] Thompson, W., Mutch, K. and Berzins, V., "Dynamic Occlusion Analysis in Optical Flow Fields", IEEE Transactions on Pattern Recognition and Machine Intelligence, vol. 7, no.4, pp. 374-383, 1985.